Nanoscale

Accepted Manuscript

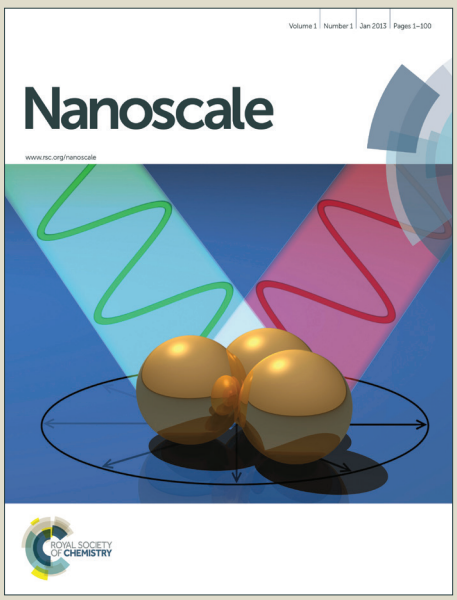

ROYAL SOCIETY OF CHEMISTRY

www.rsc.org/nanoscale

Tailoring Viscoelastic Response of Carbon Nanotubes Cellular Structure using Electric Field

Abha Misra[1] and Praveen Kumar[2]*

[1]Department of Instrumentation and Applied Physics, Indian Institute of Science, Bangalore 560012

[2]Department of Materials Engineering, Indian Institute of Science, Bangalore 560012

Abstract

Cellular structures of carbon nanotubes (CNT) are novel engineering materials finding applications due to their remarkable structural and functional properties. Here, we report the effects of electric field, one of the most frequently used stimulants for harnessing the functional properties of CNT, on the viscoelastic response, an important design consideration for the structural applications, of a cellular CNT sample. Application of electric field results in electrostriction induced large actuation in freestanding CNT samples; however, if the CNT are prohibited to expand, an electric field dependent force is exerted by the sample on the constraining platens. In addition, the above force monotonically decreases with the pre-compressive strain imposed onto the sample. The viscoelastic recovery reveals a decrease in the stress relaxation with an increase in the pre-compressive strain in both presence and absence of the electric field; however, the stress relaxation was significantly higher in the presence of electric field. A model, based on simple linear viscoelastic solid and incorporating the electric field, is developed to understand the experimental observations.

Keywords: Cellular CNT; Viscoelasticity; Recovery; Electric field; Simple linear model

*Corresponding author. Tel: +91-80-22933369. Fax: +91-80-23600472. Email: praveenk@materials.iisc.ernet.in (Praveen Kumar)

1. Introduction

Carbon nanotube (CNT) based structures in either pure form, such as cellular structure (also referred as foam, mat or turfs) or derived form, such as CNT-polymer/metal composites, possess multi-functional properties, often exhibiting excellent combination of strength, damping and shock absorption capabilities, high temperature stability, electrostriction inducted ultra-high actuation, optical and gas sensing abilities, etc. [1-12]. The inherent multifunctional properties of CNT can also be easily tailored by addition of appropriate second phase materials, such as metal-oxide nano-particles, etc. [13,14], fluid medium [15-17], chemical functional groups [18-21], etc. Due to the tunable multi-functionality and easy packaging of CNT in various forms, CNT based materials are excellent engineering materials, suited especially for applications where more than one of the above properties are exploited simultaneously, such as shock absorbing actuator arms (or, "muscles") of miniaturized robots, electric field activated "smart" switches and joints in a structure, etc. The above examples are confined to applications where the mechanical performance and the electric field induced actuation are simultaneously exploited repeatedly over extended period of time. Since, the cellular CNT are also viscoelastic showing time dependent mechanical behavior [22-25], it is imperative to study the effect of electric field on the viscoelastic response of cellular CNT before using it for any of the above highlighted applications; this forms the main goal of this study.

The viscoelastic creep and relaxation of cellular CNT and CNT-polymer composites have been extensively studied using nano-indenter and conventional mechanical testers [22-25]. In summary: (i) the CNT samples continuously accumulate strain at a constant stress exhibiting standard primary creep phase, where rapid accumulation of strain is accompanied by a decrease in the strain rate with time, followed by secondary creep phase, where the strain accumulation

occurs at a constant strain rate [22, 23], (ii) the overall stress needed to maintain a constant engineering strain first rapidly and then slowly reduces with time asymptomatically reaching a constant stress value [23, 25] and (iii) a finite stress-strain hysteresis often occurs during a loading-unloading excursion [17]. CNT shows viscoelasticity even at the room temperature, indicating that the structural integrity and the load bearing capacity of the CNT based structures would significantly evolve with time; this poses a severe reliability issue. It is generally understood that viscoelasticity in the CNT may originate from one or a combination of the following phenomenon: (i) thermally activated sliding of CNT nodes [27], (ii) partially irreversible re-orientation of CNT bundles [21, 25, 26] and (iii) sliding of CNT bundles over each other accompanied by the formation of new CNT nodes. In all of the above mechanisms of viscoelasticity in CNT, the location of an individual CNT or the collective CNT bundle changes relative to other through their energy dissipative movement.

Various quantitative models describing viscoelastic response of cellular CNT have been proposed. Mesarovic and co-workers [27, 28] modeled CNT turfs as super-compressible foam consisting of sliding CNT nodes and quantified the viscoelastic relaxation response using the Kelvin-Voigt element, i.e., the stress decayed exponentially with time. On the other hand, Xu et al. [26] modelled similar CNT structures as non-interacting coils and quantified creep recovery using a power law: $G \sim \varepsilon^{-2}$ where G is stiffness and ε is strain. While the previous two models explained the experimental results obtained through nano-indentation tests, Lattanzi et al. [23] conducted creep as well as stress-relaxation experiments on CNT samples using standard compression tests in a universal testing machine (UTM) and reported that CNT showed non-linear viscoelasticity which could be described by a power-law relationship: $\sigma(t) \sim K_{sr}t^m$ and $\varepsilon(t)$

$\sim K_{cr}t^n$, where $\sigma(t)$ and $\varepsilon(t)$ are time dependent stress and strain, respectively, K_{sr} and K_{cr} are the power-law coefficients, and m and n are dimensionless power-law exponents.

Even though the viscoelasticity in CNT is qualitatively and quantitatively understood, the effect of electric field on this phenomenon, to the best of the authors' knowledge, has yet not been studied. Since the application of electric field polarizes the CNT causing electrostriction induced actuation by altering CNT-CNT interaction[1] [7, 29-34], such a study may also help to reveal the fundamental mechanism of the viscoelasticity in cellular CNT as well as the role of van der Waals interactions in these structures. Furthermore, analysis of the effects of electric field on the viscoelasticity also requires incorporating the effect of electric field on the strengthening of cellular CNT. This makes the problem of effect of electric field on the viscoelastic behavior of CNT more intriguing and challenging. In this study, we have systematically conducted experiments to reveal the interactions between the electric field and the viscoelastic response of a cellular CNT, and proposed a phenomenological model to explain and quantify the observed interaction.

2. Experimental methods

2.1. Sample preparation

Cellular CNT samples were synthesized using chemical vapor deposition (CVD). The details of the procedure are available in reference 7 and the main steps are outlined here for continuity. Silicon di-oxide ($SiO_{2)}$ substrate was kept into a reaction zone of a tubular furnace filled with Ar

[1]Several theoretical as well as experimental works on CNT have suggested charge separation upon application of electric field; this leads to the electrostriction induced actuation in CNT [7, 29, 32-34].

gas and maintained at high temperature (825 ^{o}C). A solution of 50 mL of toluene and 1 g of ferrocene was vaporized at 200 ^{o}C and then carried into the reaction zone through Ar gas. This CVD process led to the growth of vertically aligned CNT normal to SiO_2 surface. The CVD process was continued till the height of the grown CNT structure nominally reached ~1.1 mm, following which the furnace was cooled to the room temperature. The large monolithic CNT sample was removed from the SiO_2 substrate by carefully severing it using a sharp surgical knife and then several test coupons of 4 mm length and 3 mm width were cut out from the as-grown monolithic CNT sample. Therefore, the cellular CNT test coupons were of 4 × 3 × ~1.1 mm^3 size.

Figure 1 shows representative low and high magnification images of the CNT sample as observed under a scanning electron microscope (SEM) and transmission electron microscope (TEM). As shown in Fig. 1a, although the CNT were nominally vertically aligned, they were highly entangled, forming bundles consisting of more than one intertwined CNT and CNT-CNT joints (or, CNT nodes). A CNT joint was formed where two or more CNT strands crossed each other. The high magnification image shown in Fig. 1a clearly reveals that these CNT samples were highly porous and assembled in cellular (or, foam) structure. Average density of these samples, measured by dividing the mass of a test coupon by its volume, ranged from 0.22 – 0.27 g/cm^3. Hence, these samples were only ~16 to ~20% dense (theoretical density of CNT ~1.4 g/cm^3 [35]) confirming that these CNT samples can be treated as a cellular material [36]. As shown in Fig. 1b, each CNT consisted of multiple walls (>20) and the spacing between the walls was ~0.34 nm. Hence, the cellular CNT consisted of multiwall carbon nanotubes (MWNT) hence qualifying as metallic materials.

(a) (b)

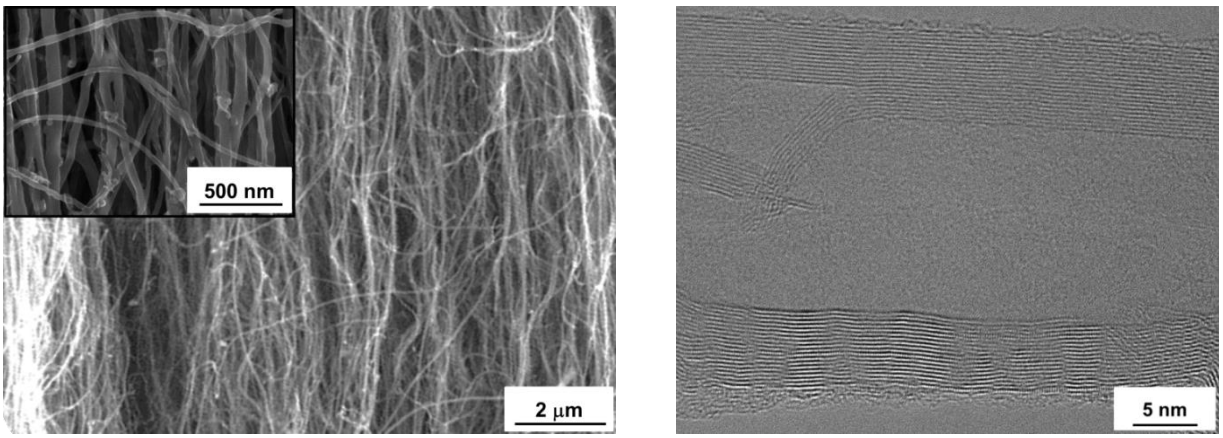

Figure 1: (a) Representative SEM micrographs showing configuration of CNT bundles and individual CNT strands in the cellular CNT samples used in this study. The SEM micrograph in the inset shows a highly magnified view. Both micrographs were taken looking along the height of the sample. (b) A high resolution transmission electron micrograph showing an individual MWCNT revealing the configuration of individual CNT walls.

2.2. Measurements of electric field actuation and stress relaxation

Figure 2a schematically shows the test set-up employed to measure the electric field induced actuation in a freestanding CNT sample. An electric field, varying from 0.5 to 2.0 kV/m, was applied along the height of the CNT sample by applying an appropriate potential difference between the two Al electrodes firmly attached to the CNT sample. It should be noted that the cellular CNT consisting of MWCNT has ultra-high electrostrictive coefficient [7]. Therefore, the electric field required for significant actuation in these CNT samples is often orders of magnitude smaller than those applied across common commercial electrostrictive materials, such as polyurethane polymers of PSX000 type, where X is 1 or 2, PVDF, polyimide-single walled CNT composites, etc. [7]. The Al electrodes of 50 μm thickness were attached to CNT surface using thin layer of high conductivity Ag-paste. The downward pressure due to the weight of an

electrode was less than 0.1% of the minimum stress measured or applied in this study. Thus, the effect of gravity on the results can be neglected. The electric field induced actuation or change in the height of the CNT samples was then measured using a high-resolution (± 0.03 μm), laser based displacement sensor (Opto NCDT 2220) mounted along direction of actuation. Synchronized outputs from the displacement sensor and the source meter (current and voltage data) (Keithley 2602A) were recorded in a master computer.

(a)

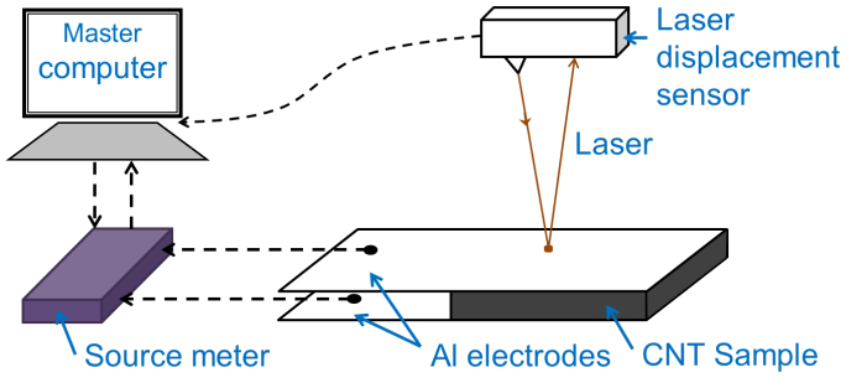

(b)

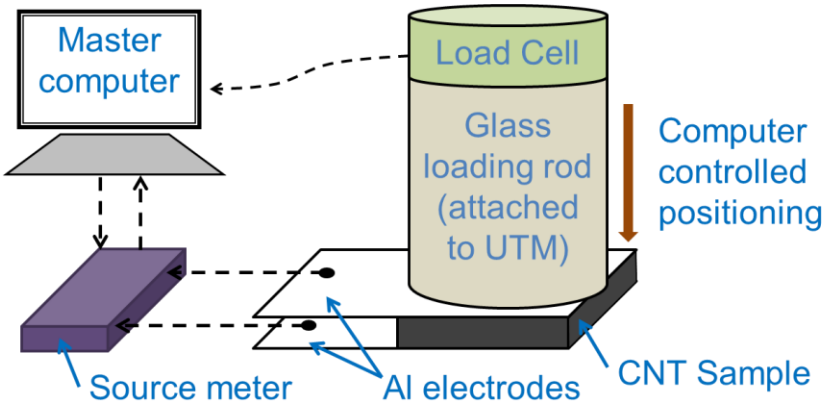

Figure 2: Schematics of the experimental set-ups for measuring (a) electric-field induced actuation in unstressed, freestanding CNT samples, and (b) stress relaxation in CNT samples pre-compressed to a fixed engineering strain. The set-up represented in (b) also allowed applying electric field.

Figure 2b shows the test set-up employed to study the stress relaxation behavior of the CNT samples with (W/) and without (W/O) electric field. The apparatus for application of electric field remained the same as that in Fig. 2a, while the CNT sample was placed in between two glass loading rods attached to a computer controlled Micro UTM (Mecmesin MultiTest 10-i). Unless otherwise stated, a 10 N load cell with a resolution of 1 mN was used to measure the force response during the mechanical tests. Before conducting an experiment, a pre-compression of 3 mN was applied to hold the sample in between the glass rods. A few experiments, where large stresses were expected, were conducted using a 100 N load cell; a note regarding such cases will be given in the figure captions. The sample was then pre-compressed to several strains of 0, 10, 20 or 30% at a strain rate of 1 s^{-1} and the evolution of the stress as a function of time (i.e., viscoelastic relaxation) was measured at various electric fields, ranging from 0 to 2 kV/m. Pulsed electric fields of various intensities were also applied in a few samples to evaluate the effect of dynamic electrical loading on the viscoelastic response of the CNT samples.

3. Experimental results

3.1. Effect of electro-mechanical coupling on strengthening of CNT samples

In order to elucidate the effects of electric field on the viscoelastic response of the cellular CNT samples, it is important to qualitatively and quantitatively understand the effects of the electro-mechanical coupling on the actuation and strengthening of the CNT samples. Figure 3a shows the electric field induced actuation in freestanding CNT samples as a function of applied electric field, as measured using the experimental set-up shown in Fig. 2a. Fig. 2a also shows the force exerted by the CNT sample onto the loading rods (or, equivalently, stress endured by the CNT samples) as a function of applied electric field when it is held at 0% strain using the experimental

set-up shown in Fig. 2b. Consistent with a previous report [7], Fig. 3a clearly shows that the electric field actuation in these cellular CNT samples was independent of the polarity of the electric field and varied as the square of the applied electric field. As suggested in earlier studies [29,32-34,37], this ultra-high actuation in the cellular CNT can be attributed to the electrostriction[2]. Interestingly, the same dependence on electric field was also observed for the stress exerted by the CNT sample on the constraining platens. This can be understood as follows: application of electric field induces a tendency of expansion in the CNT sample; however, the rigid loading rods of the UTM do not allow the sample to expand. Therefore, a compressive stress to compensate (or, nullify) the (stress free) actuation strain must be applied to the sample to maintain the same height. Since the pre-strain is zero precluding any noticeable electro-mechanical coupling effects [30] and the stress-strain relationship for the cellular CNT samples is linear in the small strain range (0 to ~2.5 %) [15,21], the stress must follow the same dependence on the electric field as that of the electric field induced actuation. This result not only confirms additional strengthening of CNT samples upon application of electric field, but also benchmarks the current experimental procedure and results with the existing literature.

[2] It should be noted that all CNT shells of a metallic MWCNT do not carry current. Actually, it has been suggested that the majority of the current passes through only the outer CNT shells [38]. Hence, although several inner CNT shells are exposed to electric field, they do not participate in flow of free electrons. These non-participating inner CNT shells of a metallic MWCNT may get polarized, leading to an overall electric field induced actuation, while the free electrons flow through the outer shells of the MWCNT. Since the electrostriction induced strain is proportional to the overall polarization of a material, the overall electric field actuation of MWCNT can be expected to significantly increase if the number fraction of CNT shells not participating in flow of free-electrons increases.

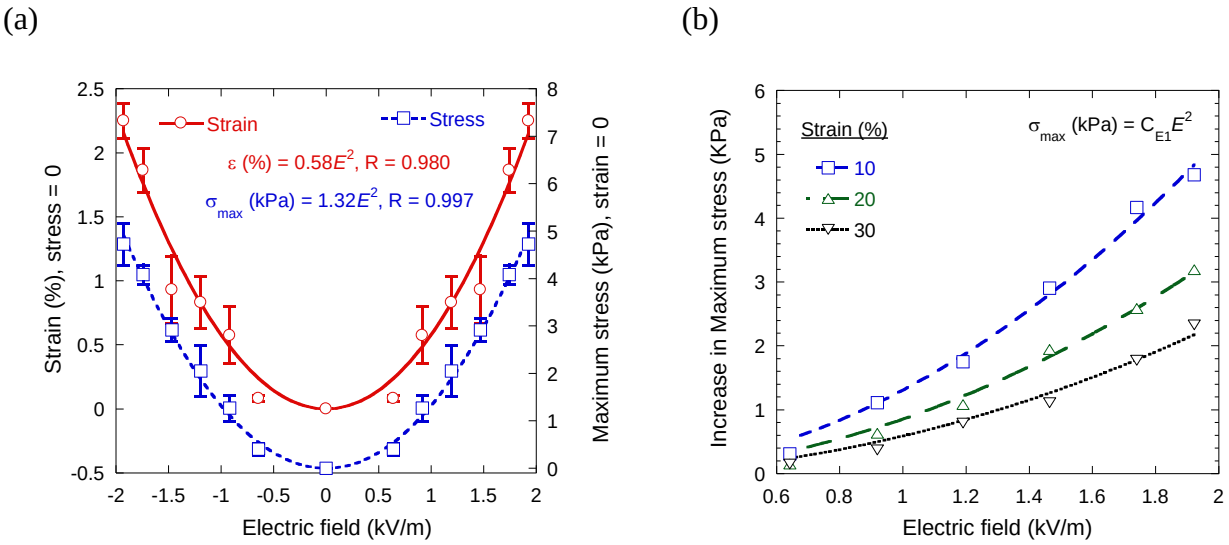

Figure 3: (a) Variation of the electric field induced strain in the unstressed freestanding CNT sample and the additional stress that needs to be applied onto the sample to maintain zero macroscopic strain as a function of the electric field. *R* is the curve fitting parameter. (b) Variation of the maximum stress required to maintain a constant pre-compressive strain as a function of the electric field. The curve fitting parameter for the equation shown in (b) was >0.99 for all pre-strain values. The load was measured using 10 N load-cell.

Figure 3b shows the effect of non-zero pre-compressive strain on the electric field induced increase in the maximum stress exerted by the loading platens on the CNT samples. As shown in Fig. 3b, irrespective of the pre-strain, the maximum stress, σ_{max} that additionally must be exerted onto the CNT sample to nullify the electric field induced actuation increased non-linearly (quadratic) with the electric field. Furthermore, Fig. 3b also reveals that the value of the required additional maximum stress at an electric field to balance the actuation strain reduced monotonically with the pre-compressive strain. This suggests that the electric field induced strengthening decreased with the pre-strain value and this may be attributed to the enhanced buckling of CNT strands and bundles once they are pre-compressed to high strain [28]. In summary, the stiffness of the CNT samples increased upon application of electric field, but the

relative increase decreased with the imposed pre-compressive strain. It should be noted that coupling between the strain (or, pre-stress) and the electric field affects the polarization in CNT and hence the actuation strain [29, 30]. However, the contribution of the above mentioned electro-mechanical coupling on the actuation and hence strengthening is not significant in this study. Therefore, the electro-mechanical coupling effects have been neglected in this study; this assumption also aids to the mathematical simplicity.

Figure 4a shows the variation in the stress required to constrain a cellular CNT sample at a pre-strain of 0% as the electric field was varied in a pulsed fashion. Figure 4b shows a magnified version of Fig. 4a and Figure 4c summarizes various parameters, such as jump in stress ($\Delta\sigma$), maximum stress at an applied electric field (σ_h) and the minimum stress value attained after switching off the electric field (σ_l). As shown in Figs. 4a and 4b the stress increased upon application of an electric field; however, there was a significant lag between the electric field switching and the stress. The stress first increased rapidly upon switching on the electric field and then it reached a maximum value asymptotically[3]. The lag in the stress value can be attributed to the lag between the electric field and the induced actuation strain, which, as discussed earlier, arises due to the surface charge generation and polarization; the lag may be further compounded due to the capacitive nature of the cellular CNT [7, 31]. Furthermore, the viscoelastic nature of CNT may also additionally contribute to the lag between the electric field application and the realization of the actuation strain.

[3] It should be noted that the stress reported in Fig. 3 corresponds to the maximum stress within 10 minutes of the application of electric field.

(a)

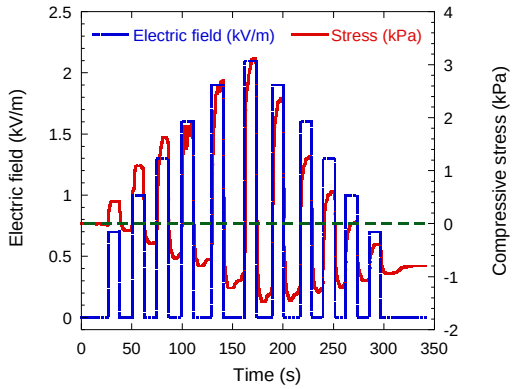

(b)

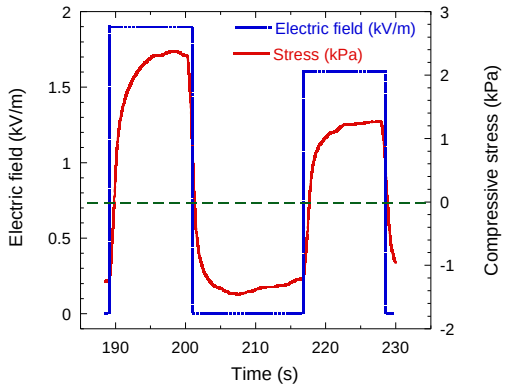

(c)

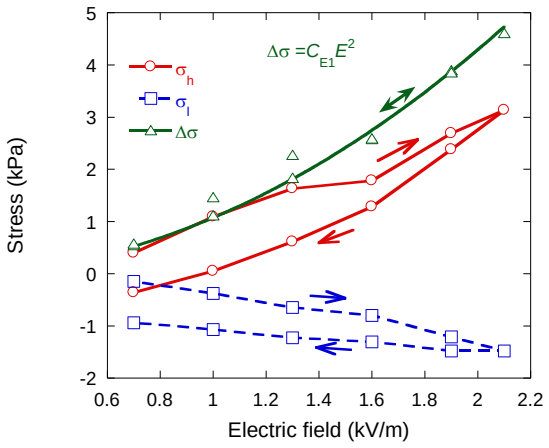

Figure 4: (a) Variation of stress as a function of varying pulsed electric field, as measured by the set-up shown in Fig. 2b, (b) a magnified view of (a), and (c) variation in the stress jump ($\Delta\sigma$), the highest stress level upon application of electric field (σ_h), and the lowest stress level upon switching off the electric field (σ_l) as function of the applied electric field. The plot in (c) is derived from (a). The arrows on the curves in (c) indicate the sequence of the events.

Careful observation of Fig. 4 also reveals the following:

i. The stress in the sample did not instantaneously become zero upon switching off the electric field and as a matter of fact, it transitioned from compressive to tensile. The tensile stress can be attributed to a reduction in the height of the sample due to the compressive stress generated upon application of electric field. Also, due to the compressive stress, the van der Waals interaction between the CNT sample and the flat glass platen was enhanced leading to "attachment" of CNT sample and the glass plates. As the electric field was switched off, the

shortened CNT sample pulled the glass rods down leading to a tensile stress in the CNT sample.

ii. The tensile stress upon switching off the electric field reached a maximum following which it started to reduce (Figs. 4a and 4b). The reduction in the stress can be attributed to the viscoelastic relaxation.

iii. The change in the stress value upon application of electric field, $\Delta\sigma$, during the pulse cycling appears to be history independent. Furthermore, consistent with the observation in Fig. 3a, the change in the stress upon switching on the electric field remains proportional to the square of the electric field.

iv. As expected, the maximum compressive stress (σ_h) monotonically increased with the applied electric field, and consistent with the explanation provided above, the maximum tensile stress upon switching off the electric field (σ_l) also increased with the maximum compressive stress (Fig. 4c). However, there was a finite stress-stain hysteresis: σ_h and σ_l did not become zero at the end of the voltage pulse cycling (Fig. 4c) and the final stress value appears to have saturated at a non-zero tensile value (Fig. 4a). It suggests that the repetitive voltage cycling may cause permanent deformation in CNT samples that may recover, if at all, only after very long time. However, the effect of electric field on the strengthening mechanism of CNT, i.e., the value of $\Delta\sigma$, was history independent.

3.2. Stress relaxation in CNT samples

Figure 5a shows the stress relaxation behavior of a cellular CNT sample in the absence of electric field. The sample was pre-strained to various engineering strains and stress relaxation was measured for 10 minutes using the experimental set-up shown in Fig. 2b. As shown in Fig.

5a, the force applied on the sample rapidly increased upon application of strain reaching a maximum value. Once the maximum stress was reached, the stress initially relaxed almost instantly (region I, inset of Fig. 5a), then at a rapid rate during a short duration (region II, inset of Fig. 5a) followed by a gradual decay over a long period of time (region III, inset of Fig. 5a). At the termination of region III, the stress asymptotically approached a constant value, which will be henceforth termed as saturation stress. Same tests were also conducted in the presence of electric field and similar salient features for the stress relaxation were observed. It should be noted that pre-loading in this study were conducted at only one strain rate (1 s^{-1}). Since the cellular CNT is a viscoelastic material, the stress value following the initial ramp loading as well as the microstructure of the sample (i.e., configuration of CNT strands and bundles, and mutual interactions amongst CNT strands) depend on this strain ramp rate [39]. Interestingly, a recent report [40] showed insignificant effect of strain rate, ranging from 10^{-4} to 10^{-1} s^{-1}, on the stress-strain behavior and total energy dissipated by the cellular CNT. In either case, although the exact value of stresses in Fig. 5 (and other similar graphs showing stress relaxation) may depend on the strain ramp rate, the stress relaxation behavior as shown in Fig. 5 is representative of the cellular CNT and it clearly demonstrates the effect of electric field on its viscoelastic response.

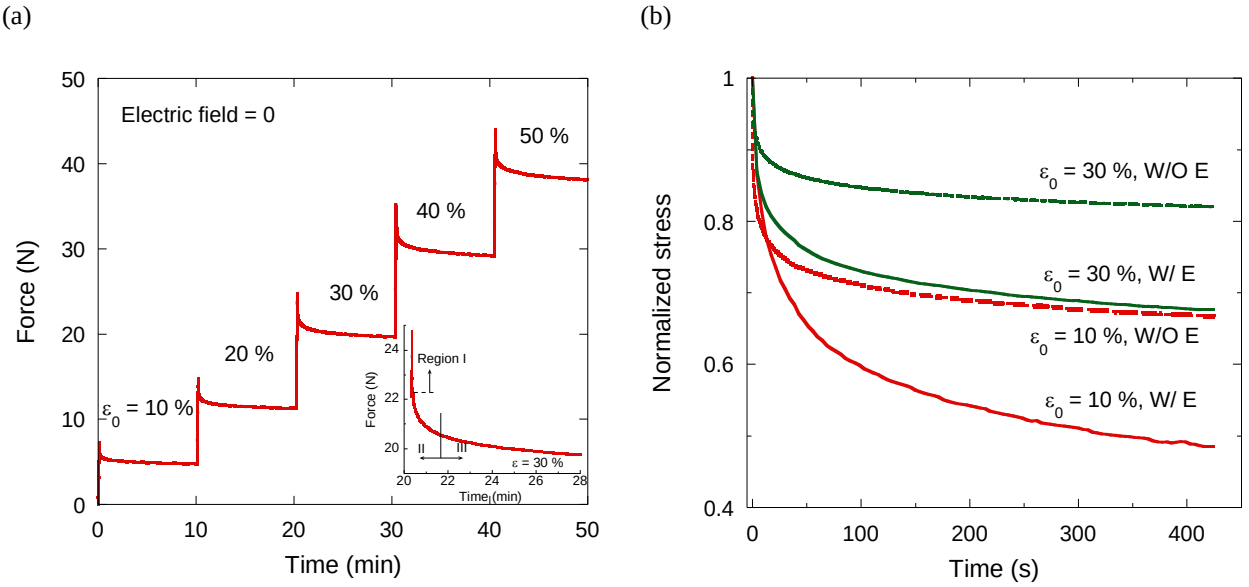

Figure 5: The stress relaxation as registered in a representative CNT sample compressed to various pre-compressive strains: (a) with no electric field, and (b) under an electric field corresponding to ~1.35 kV/m. The inset in (a) shows a magnified view of one of the stress relaxation curves (corresponding to a pre-strain, ε_0, of 30%). In (b) the symbols W/O and W/ represent the condition of without and with electric fields, respectively.

Figure 5b shows a few representative stress relaxation curves of cellular CNT samples in the absence (W/O) and the presence (W/) of electric field. The stress relaxation is represented in terms of normalized stress, calculated by dividing σ(t) by the maximum stress attained following a stress jump (i.e., the peak of the region I), and the time axis for various pre-strains were shifted to zero so that all curves start from the same point. Representing the data shown in Fig. 5a in the form of Fig. 5b allows direct observation of the effects of pre-strain and electric field on the stress relaxation behavior without getting affected by the initial stress level (which depended on both the pre-strain value and the applied electric field, and as mentioned earlier, will also depend on the strain ramp rate). Fig. 5b readily reveals the following salient features of the viscoelastic behavior of cellular CNT samples: (i) irrespective of the electric field application, the span of

region II was not only larger, but also the saturation stress was lower for the cellular CNT samples pre-strained to a smaller compressive strain, and (ii) irrespective of the pre-strain value, the span of region II was not only considerably larger, but also the saturation stress was lower in the presence of electric field. In summary, the effect of electric field on the viscous stress relaxation was contrary to the effect of pre-compression strain.

Figure 6 shows the stress-relaxation of a cellular CNT sample pre-compressed to two different strain values in the presence of pulsed electric field or under dynamic electric field loading. The magnitude of electric pulses was increased in an interval of 0.02 V, which corresponds to an electric field of ~20 V/m, and the electric field was applied in the same fashion (magnitude and frequency) for both the conditions shown in Fig. 6. Consistent with Fig. 3 and 4, the stress applied on the sample by the loading rods to maintain the same macroscopic strain increased upon applying the electric field and the increment in the stress monotonically increased with the magnitude of the electric field. However, the increment in the stress was significantly smaller if the sample was pre-compressed to higher strain values; this is consistent with the findings shown in Fig. 3b. Fig. 6 also reveals that the stresses drops below the stress value as expected for the condition of no electric field during the stress relaxation (shown by dotted line in Fig. 6). This is consistent with Fig. 5b that the stress relaxation occurring in the presence of (pulsed) electric field was faster as compared to that in the absence of electric field. This led to a significant drop in the stress level once the electric field was turned off. Similarity in the results obtained during the dynamic and the static electric field loading suggests that the fundamental mechanism governing the effect of electric field on the viscoelasticity in the CNT samples did not depend on the nature of electric field.

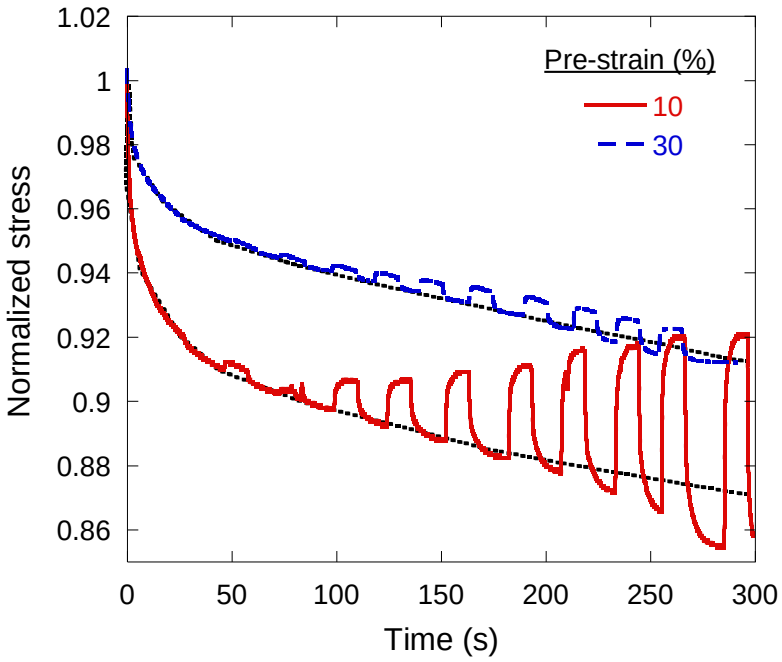

Figure 6: Variation of the normalized stress as a function of the time after application of the "instantaneous" pre-compressive strain. The pulse voltage increased by 0.02 V in the sequence of 0.07, 0.09, 1.1, etc. The dotted line represents stress relaxation if electric field was not applied.

4. Discussion

4.1. Three regions (stages) of stress-relaxation

As shown in Fig. 5a, the stress relaxation of cellular CNT showed three regions (or, stages), each region was identified by the apparent rate of stress relaxation. Existence of the three distinct regions can be rationalized as follows. In open cell foam structures compressed under quasi-static conditions and at moderately high strain rates, the deformation field can be inhomogeneous where the maximum deformation is concentrated near the sample ends [41]. Since inhomogeneous stress (or, strain) field with large stress (or, strain) gradient in a body with uniform composition is a non-equilibrium state, the stress field in the cellular CNT must evolve

to become homogenous. During this homogenization process, the highly deformed regions compress the neighboring regions and reduce the local strain at the expense of straining of the neighboring regions. Since cellular CNT samples show highly non-linear stress-strain behavior where the stresses rapidly increase with strain [15], the aforementioned homogenization of stress (or, strain) field would lead to a dramatic decrease in the macroscopic stress; this mechanism is suggested to be responsible for the almost instantaneous decrease in the stress as observed in region I (Fig. 5a, inset). Furthermore, Fig. 5a indicates that the drop in stress value in region I increased with the pre-strain value. This is consistent with the proposed understanding (of almost instantaneous drop in the stress due to homogenization of strain field) as the stress-strain behavior of the cellular CNT samples becomes severely non-linear at higher strains and hence a small decrease in the local strain in the high strain regime will cause dramatically large reduction in the stress.

Regions II and III represent the usual viscoelastic relaxation processes where rearrangement of the local microstructure occurs uniformly throughout the sample in response to a uniform stress-field. Since the stress field is large in the beginning of the relaxation process, the rate of microstructural rearrangement is rapid in the initial stage leading to fast stress relaxation (i.e. region II). As the stress reduces, the driving force for the rearrangement reduces and the stress relaxation process slows down and the stress asymptotically reaches an equilibrium value where the stress field, although non-zero, is too small to drive any microstructural rearrangement (region III). Thus, the saturation stress value should scale with the internal static friction between CNT strands and nodes, which must be overcome to cause *viscosity* driven microstructural rearrangement in CNT samples.

As shown in Fig. 5b, the span of region II and the total stress recovery at low pre-strain and in the presence of electric field were significantly larger indicating the effect of pre-strain and the electric field on viscoelastic response are opposite and these can be tuned to nullify the effects of each other. These observations can be rationalized as follows: As the cellular CNT sample is compressed to higher strains, the sample become denser and also, the volume fraction of buckled CNT strands and bundles increases [42], both of which lead to an increase in the total CNT-CNT overlap area. Therefore, the total "frictional" forces opposing the stress relaxation increases with the compressive strain. In addition, buckling of CNT strands reduces the net elastic driving force for the recovery. Therefore, at higher compressive strains, a smaller driving force for microstructural rearrangement is available leading to a small span of region II and a higher saturation stress. On the other hand, the stiffness of the CNT samples increases (Fig. 3) [30] and the buckling of CNT strands under compression dramatically reduces [43] in the presence of electric field. The net effects of these are increase in the elastic driving force for recovery and reduction in the buckling induced CNT-CNT overlap area. Also, the electric field induced polarization of CNT strands results in Columbic repulsion between neighboring CNT strands [7], the CNT-CNT overlap area may further reduce. The existence of aforementioned Columbic repulsion was confirmed by observation of expansion of cellular CNT samples in the transverse direction upon application of electric field along the height of the sample [7]. Hence, due to an increase in elastic stress and a decrease in the frictional forces opposing microstructural rearrangement, large stress recovery occurs in the presence of an electric field.

4.2. Quantification and modeling of effect of electric field on stress-relaxation

Fig. 5b reveals an extremely sharp drop in the stress values in short duration followed by a long gradual decrease. Such type of curves often indicates an exponential decay law and may not be fitted readily using simple power law. Since the Maxwell element represents the viscous and the elastic components in iso-stress configuration whereas the Kelvin-Voigt element represent these two components in iso-strain configurations, usage of either of these two elements represent the two extremes of viscoelastic behavior. Therefore, it is appropriate to use the standard linear solid (SLS) model, which combines both the Maxwell and the Kelvin-Voigt elements in the fashion shown in Figure 7 [44][4].

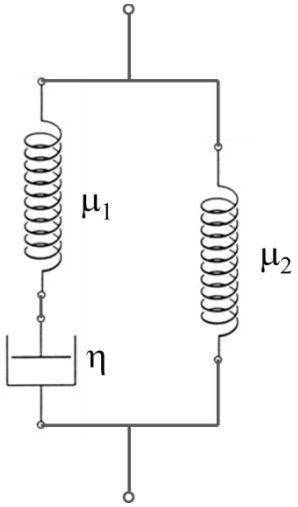

Figure 7: A schematic representation of a 3 parameter, simple linear viscoelastic model. The stiffness of the two springs are μ_1 and μ_2 and the viscosity of the dash-pot is η.

[4] Stretched exponential function or Kohlrausch, Williams, Watts (KWW) model [44] may fit the observed experimental data better than the standard linear model (Supplemental Material 1); however, the standard linear model is chosen in this work for the associated mathematical simplicity and ease of physical interpretation of different terms.

For the simple linear solid model, the effective modulus as a function of time, μ(t), is given as follows [44]:

$$\mu(t) = \mu_2 + \mu_1 e^{-(t/\tau)} \quad (3)$$

where μ_1 and μ_2 are defined as in Fig. 7, t is time and τ is the relaxation time defined as η/μ_1, where η is the effective viscosity of the material (Fig. 7). Expression for the macroscopic stress σ(t) can derived by multiplying both sides of Equation (3) by the macroscopic pre-strain, ε_0, at which the stress relaxation experiment was conducted:

$$\sigma(t) = \varepsilon_0\left(\mu_2 + \mu_1 e^{-(t/\tau)}\right) \quad (4)$$

Dividing both sides of Equation (4) by the initial stress (i.e., σ at $t = 0$) gives the following expression for the normalized stress, σ_n, as a function of time:

$$\sigma_n(t) = \frac{\mu_2 + \mu_1 e^{-(t/\tau)}}{\mu_1 + \mu_2} = 1 - M_1\left(1 - e^{-(t/\tau)}\right) \quad (5)$$

where M_1 is constant equal to $\mu_1/(\mu_1+\mu_2)$. M_1 represents total stress relaxation so that the normalized saturation stress is equal to $1\text{-}M_1$. As shown in Fig. 5b as well as previously explained, the value of M_1 for cellular CNT sample depends on the pre-strain and the electric field. It should be noted that the form of Eq. (5) is independent of the pre-strain and hence justifies plotting of the stress-relaxation data in form of Fig. 5b.

A curve fitting exercise using Equation (5) over the data shown in regions II and III of Fig. 5b (i.e., the data representing only viscoelastic stress relaxation) was conducted (refer to Supplemental Material 1 for curve fitting). Figure 8 shows the variation of M_1 and τ as a function of pre-strain values for both the cases of with and without electric field. As shown in Fig. 8, both

M_1 and τ monotonically decreased with pre-strain, but their values dramatically increased in presence of electric field. This is consistent with the observation that the saturation stress, which scales with 1-M_1, increased with increase in pre-strain and decreased upon application of electric field. Also, τ represents the span of the stress-relaxation duration such that higher is its value, the longer is the duration of the stress relaxation. Therefore, a decrease in the value of τ with strain is consistent with smaller span of region II for the samples pre-compressed to larger strains and an increase in its value upon application of electric field is consistent with an increase in span of region II for the samples tested in the electric field.

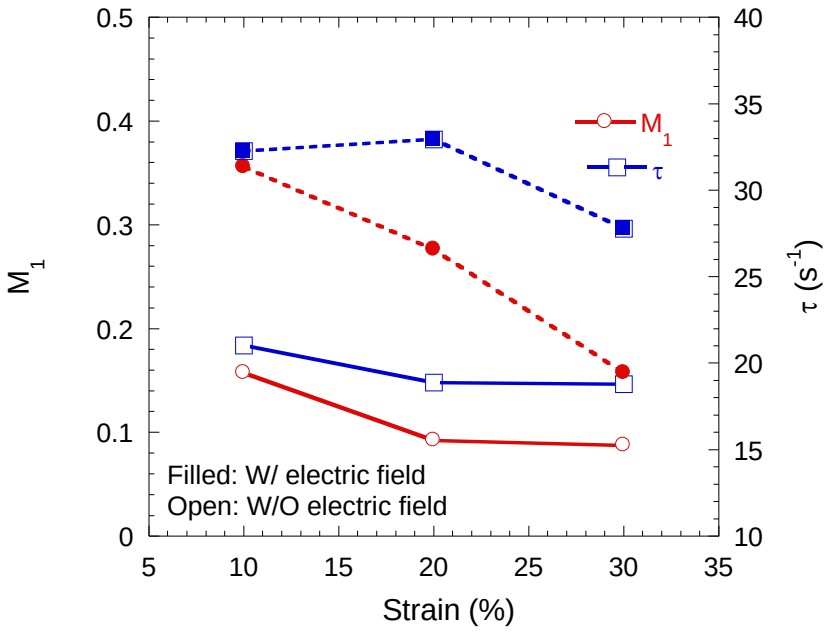

Figure 8: Variation of M_1 and τ as functions of the pre-strain value. The symbols W/ and W/O represent with and without electric field, respectively. The data shown here was derived through curve fitting of data shown in Fig. 5b (Supplemental material). The curve fitting parameter was >0.96.

According to the assumptions of standard linear model (Fig. 7), the viscosity of the dash-pot element, η, should scale with the ratio of M_1 and τ. Using the definition of τ ($=\eta/\mu_1$) and Equations 2 and 4, the increase in the effective viscosity of cellular CNT sample in the electric field can be given as follows:

$$\frac{\eta_E}{\eta_0} = \frac{\tau_E M_{1,E}}{\tau_0 M_{1,0}} \left(1 + \frac{C_{E1} E^2}{\sigma_0} \right) \quad (6)$$

where the subscripts E and 0 denote with and without electric field conditions and constant C_{E1} represents strengthening due to the electric field. As shown in Fig. 9, values of both τ and M_1 increased upon application of electric field and quantity in the parentheses in right hand side of Equation (6), which is actually ratio of stresses in the presence and in the absence of electric field at the same macroscopic strain, will always be greater than 1 (Fig. 3). Therefore, the effective viscosity of cellular CNT will always increase upon application of electric field. Since viscosity represents the resistance (or friction) against the mobility of molecules or atoms of a medium, the observed increase in the apparent viscosity of CNT samples may originate from the Columbic repulsion between CNT strands in presence of electric field. Interestingly, as the viscosity of a material also represents its ability to endure the shear load induced gradient in the flow (or, deformation), the deformation field in the cellular CNT sample should become more uniform in the presence of electric field. This suggests suppression of buckling, which often starts from one end of the sample [42], in presence of electric field; this is consistent with a recent report [43].

5. Conclusions

1. The cellular CNT samples showed significant electric field induced actuation, which can be attributed to electrostriction. The stress required to constrain the sample from actuating or expanding increases monotonically with the electric field.
2. Significant stress relaxation occurs in the cellular CNT samples. The saturation stress is small if the pre-compression strain is small or if the electric field is switched on. The span over which stress relaxation occurs is large in the samples pre-compressed to small strains or if the electric field is switched on.
3. Although the sample can deform permanently under repetitive application of pulsed electric field, the change in the maximum stress due to application of electric field is history independent and does not depend on the extent of the stress relaxation. Also, the effect of electric field on viscoelastic response of CNT remains the same under static and dynamic electric field.
4. A simple standard linear solid model incorporating Maxwell as well as Kelvin-Voigt elements can be used to understand and interpret the stress relaxation behavior of cellular CNT sample in the presence as well as in the absence of electric field.

Acknowledgements

PK would like to acknowledge financial support from Council of Scientific and Industrial Research, India under the financial grant # CSIR 0366. Authors would like to thank Mr. Robin Singla of Kurukshetra University (India) for help with the experimental work.

References:

1. Qian D, Wagner G J, Liu W K, Yu M -F and Ruoff R S 2002 *Appl. Mech. Rev.* **55** 495.
2. Bradford P D, Wang X, Zhao H and Zhu Y T 2011 *Carbon* **49** 2834.
3. Yakobson B I and Avouris P 2001 *Topics in Appl. Phys.* **80** 287.
4. Misra A, Greer J R and Daraio C 2009 *Adv. Mater.* **21** 334.
5. Shastry V V, Ramamurty U and Misra A 2012 *Carbon* **50** 4373.
6. Kiran M, Ramamurty U and Misra A 2013 *Nanotechnology* **24** 015707.
7. Gowda P, Kumar P, Tripathi R and Misra A 2014 *Carbon* **67** 546.
8. Suri A and Misra A 2013 *Nanotechnology* **24** 105501.
9. Gowda P, Suri A, Reddy S K and Misra A 2014 *Nanotechnology* **25** 025708.
10. Baughman R H, Cui C, Zakhidov A A, Iqbal Z, Barisci J N, Spinks G M, Wallace G G, Mazzoldi A, De Rossi D, Rinzler A G, Jaschinski O, Roth S and Kertesz M. 1999 *Science* **284** 1340.
11. Fennimore A M, Yuzvinsky T D, Han W Q, Fuhrer M S, Cumings J and Zettl A 2003 *Nature* **424** 408.
12. Barone P W, Baik S, Heller D A and Strano M S 2005 *Nature Materials* **4** 86.
13. Costa P M F J, Coleman K S and Green M L H 2005 *Nanotechnology* **16** 512.
14. Gowda P, Ramamurty U and Misra A 2014 *Appl. Phys. Lett.* **104** 101911.
15. Reddy S K, Suri A and Misra A 2013 *Appl. Phys. Lett.* **102** 241919.
16. Misra A, Kumar P, Raney J R, Singhal A, Lattanji L and Daraio C 2014 *Appl. Phys. Lett.* **104** 221910.
17. Reddy S, Mukherjee A and Misra A 2014 *Appl. Phys. Lett.* **104** 261906.
18. Zhang T, Mubeen S, Myung N V and Deshusses M A, 2008 *Nanotechnology* **19** 332001.
19. Abdelhalim A, Abdellah A, Scarpa G and Lugli P 2014 *Nanotechnology* **25** 055208.

20. Zhang T, Nix M B, Yoo B -Y, Deshusses M A and Myung N V 2006 *Electroanalysis* **18** 1153.
21. Misra A, Raney J R, Craig A E and Daraio C 2011 *Nanotechnology* **22** 425705.
22. Zhang Q, Lu Y C, Du F, Dai L, Baur J and Foster D C 2010 *J. Phys. D: Appl. Phys.* **43** 315401.
23. Lattanzi L, Raney J R, De Nardo L, Misra A. and Daraio C 2012 *J. Appl. Phys.* **111** 074314.
24. Xu M, Futaba D N, Yumura M and Hata K 2011 *Adv. Mater.* **23** 3686.
25. Qiu A, Fowler S P, Jiao J, Kiener D and D F Bahr 2011 *Nanotechnology* **22** 295702.
26. Xu M, Futaba D N, Yumura M and Hata K 2011 *Nano letters* **11** 3279.
27. Mesarovic S Dj, McCarter C M, Bahr D F, Radhakrishnan H, Richards R F, Richards C D, McClain D and Jao J 2007 *Scripta Mater.* **56** 157.
28. Radhakrishnan H, Mesarovic S Dj, Qiu A and Bahr D F 2013 *Int. J. Solids Struct.* **50** 2224.
29. Guo W and Guo Y 2003 *Phys. Rev. Lett.* **91** 115501.
30. Jagtap P, Gowda P, Das B and Kumar P 2013 *Carbon* **60** 169.
31. Madden J D W, Barisci J N, Anquetil P A, Spinks G M, Wallace G G, Baughman R H and Hunter I W 2006 *Adv. Mater.* **18** 870.
32. El-Hami K and Matsushige K 2005 *Ultramicroscopy* **105** 143.
33. Guo Y and Guo W 2003 *J. Phys. D* **36** 805.
34. Wang Z and Philippe L 2009 *Phys. Rev. Lett.* **102** 215501.
35. Collins P G and Avouris P 2000 *Scientific Amer.* **283** 62.
36. Gibson L J and Ashby M F, "Cellular Solids: Structure and Properties", Cambridge University Press, Cambridge, UK (1997).
37. Fraysse J, Minett A I O and Jaschinski G S 2002 *Carbon* **40** 1735.

38. Collins P G, Arnold M S and Avouris P 2001 *Science* **292** 706

39. Pathak S, Lim E J, Abadi P S S, Graham S, Cola B A and Greer J R 2012 *ACS Nano* **6** 2189

40. J R Raney J R, Fraternali F and Daraio C 2013 *Nanotechnology* **24** 255707

41. Lee S, Barthelat F, Moldovan N, Espinosa H D and Wadley H N G 2006 *Int. J. Solids Struct.* **43** 53.

42. Cao A, Dickrell P L, Ghasemi-Nejhad M N, Sawyer W G and Ajayan P M 2005 *Science* **310** 1307.

43. Jagtap P, Reddy S K and Kumar P, Tailoring energy absorption capacity of carbon nanotube foams by application of electric field, submitted (2014).

44. Lakes R, "Viscoelastic Materials", Cambridge University Press, Cambridge, UK (2009)

Supplemental Material 1: Curve fitting exercise on data shown in Fig. 5b

- The curve fitting exercise conducted using Equation (5): M1 = M_1, M2 = τ and M0 = t

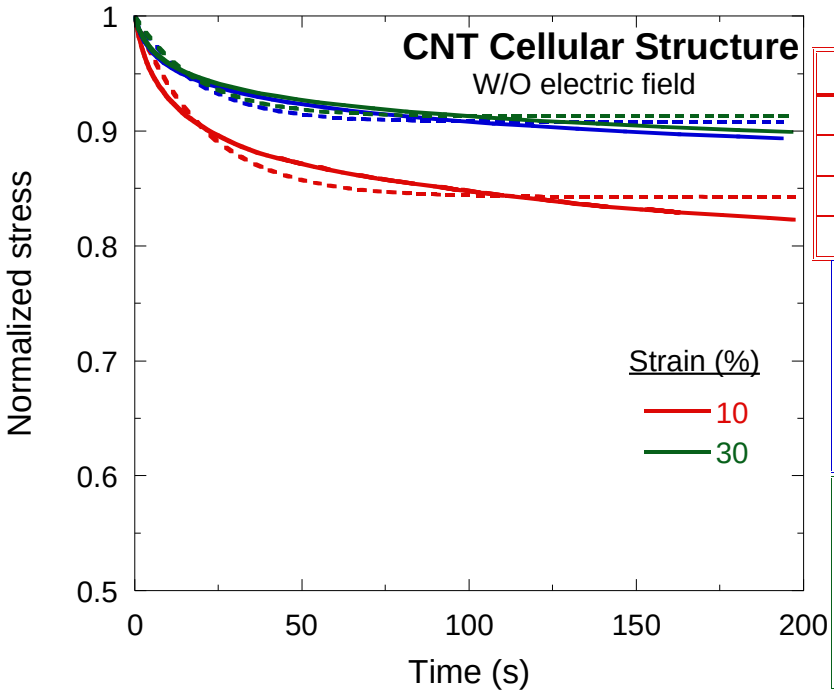

y = 1-M1*(1-exp(-M0/M3))	
	Value
m1	0.15731
m3	21.047
R	0.97882

y = 1-M1*(1-exp(-M0/M3))	
	Value
m1	0.092051
m3	18.89
R	0.97392

y = 1-M1*(1-exp(-M0/M3))	
	Value
m1	0.087377
m3	18.789
R	0.97467

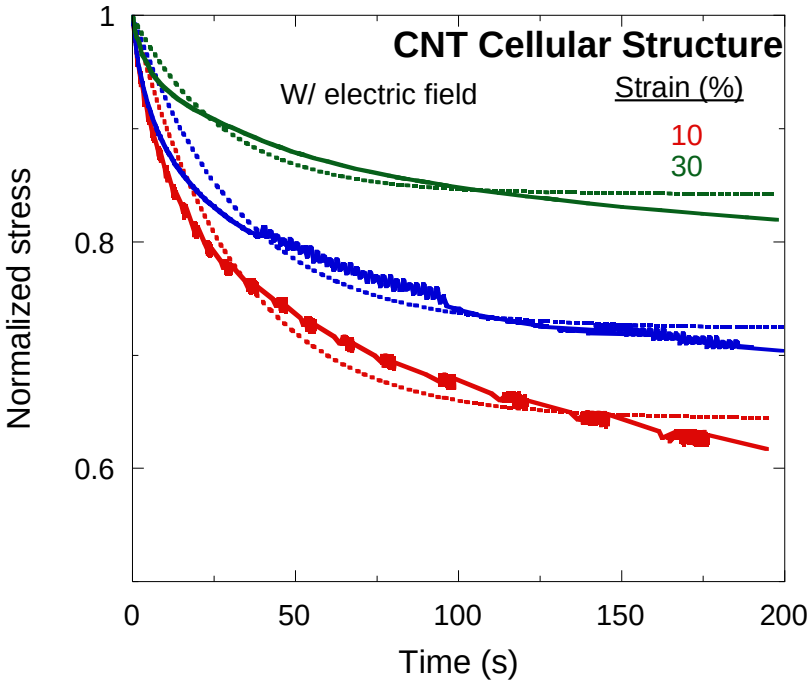

y = 1-M1*(1-exp(-M0/M3))	
	Value
m1	0.35612
m3	32.261
R	0.9707

y = 1-M1*(1-exp(-M0/M3))	
	Value
m1	0.27606
m3	32.933
R	0.96218

y = 1-M1*(1-exp(-M0/M3))	
	Value
m1	0.1577
m3	27.785
R	0.97419

- The curve fitting exercise conducted using the KWW model: M1 = M_1, M2 = τ, M3 = β and M0 = t

$$\sigma_n(t) = 1 - M_1\left(1 - e^{-\left(\frac{t}{\tau}\right)^{\beta}}\right)$$

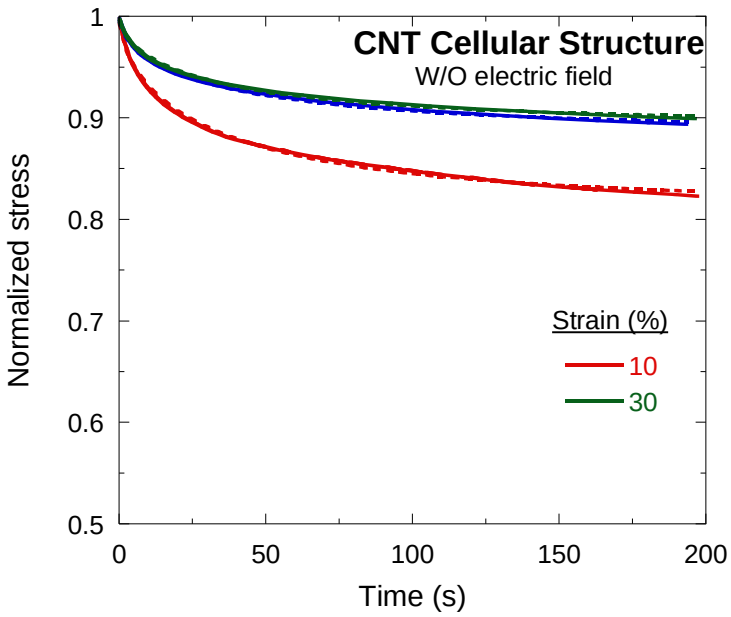

y = 1-M1*(1-exp(-(M0/M2)^M3)...	
	Value
m1	0.18397
m2	35.972
m3	0.5979
R	0.99868

y = 1-M1*(1-exp(-(M0/M2)^M3)...	
	Value
m1	0.11144
m2	36.679
m3	0.59171
R	0.99879

y = 1-M1*(1-exp(-(M0/M2)^M3)...	
	Value
m1	0.10475
m2	35.416
m3	0.59556
R	0.99885

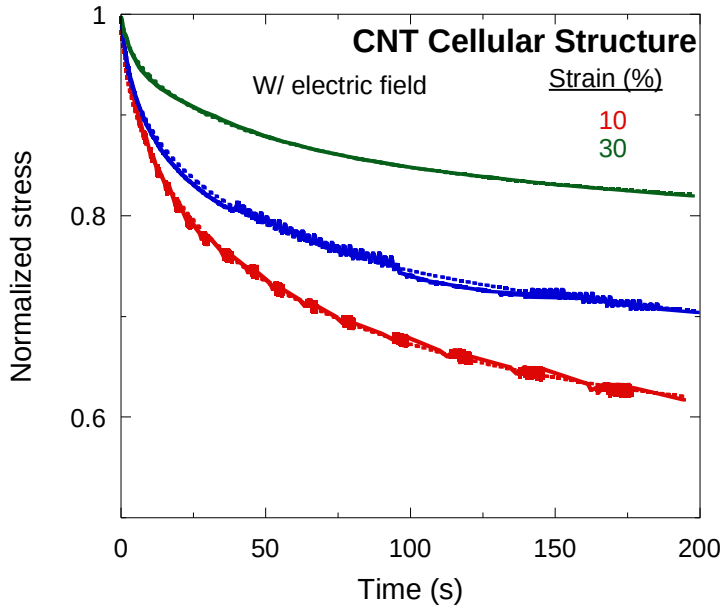

y = 1-M1*(1-exp(-(M0/M2)^M3)...	
	Value
m1	0.43835
m2	56.8
m3	0.56511
R	0.9985

y = 1-M1*(1-exp(-(M0/M2)^M3)...	
	Value
m1	0.34324
m2	56.87
m3	0.53429
R	0.99662

y = 1-M1*(1-exp(-(M0/M2)^M3)...	
	Value
m1	0.21382
m2	68.301
m3	0.5633
R	0.99946